




## Open Archive Toulouse Archive Ouverte

OATAO is an open access repository that collects the work of Toulouse researchers and makes it freely available over the web where possible

This is an author's version published in: <http://oatao.univ-toulouse.fr/21622>

**Official URL:** <https://doi.org/10.1016/j.ces.2015.04.015>

### To cite this version:

Daniel-David, Delphine and Guerton, Fabrice and Dicharry, Christophe and Torr , Jean-Philippe  and Broseta, Daniel *Hydrate growth at the interface between water and pure or mixed CO<sub>2</sub>/CH<sub>4</sub> gases: Influence of pressure, temperature, gas composition and water-soluble surfactants.* (2015) *Chemical Engineering Science*, 132. 118-127. ISSN 0009-2509

Any correspondence concerning this service should be sent to the repository administrator: [tech-oatao@listes-diff.inp-toulouse.fr](mailto:tech-oatao@listes-diff.inp-toulouse.fr)

# Hydrate growth at the interface between water and pure or mixed CO<sub>2</sub>/CH<sub>4</sub> gases: Influence of pressure, temperature, gas composition and water-soluble surfactants

Delphine Daniel-David, Fabrice Guerton, Christophe Dicharry, Jean-Philippe Torr , Daniel Broseta\*

Laboratoire des Fluides Complexes et leurs R servoirs Univ Pau and Pays Adour, 64013 Pau Cedex, France

- Hydrate growth is observed from experiments with water drops and CH<sub>4</sub>/CO<sub>2</sub> gases.
- Hydrates most often form low permeable crusts at water/gas interfaces.
- Anionic surfactants such as SDS or AOT promote CH<sub>4</sub> hydrates but not CO<sub>2</sub> hydrates.
- Insight is given into the capillary driven hydrate growth observed with SDS and AOT.

*Key words:*  
CO<sub>2</sub>/CH<sub>4</sub> hydrates  
Hydrate growth  
Hydrate promoters  
Surfactants

The morphology and growth of gas hydrate at the interface between an aqueous solution and gaseous mixtures of CO<sub>2</sub> and CH<sub>4</sub> are observed by means of a simple experimental procedure, in which hydrate formation is triggered at the top of a sessile water drop by contact with another piece of gas hydrate and the ensuing hydrate growth is video monitored. The aqueous solution is either pure water or a solution of a nonionic or anionic surfactant at low concentration (in the 100–1000 ppmw range). In agreement with previously published data, hydrates formed from pure water and aqueous solutions of non ionic surfactant grow rapidly as a low permeable polycrystalline crust along the water/gas interface, which then inhibits further growth in a direction perpendicular to the interface. Lateral growth rates increase strongly with subcooling and CO<sub>2</sub> content in the gas mixture. Similar lateral growth rates, but varying morphologies, are observed with the non ionic surfactants tested. In contrast, the two anionic surfactants tested, sodium dodecyl sulfate (SDS) and dioctyl sodium sulfosuccinate (AOT), promote in the presence of CH<sub>4</sub> (but not in the presence of CO<sub>2</sub>) a rapid and full conversion of the water drop into hydrate through a ‘capillary driven’ growth process. Insights are given into this process, which is observed with AOT for an unprecedented low concentration of 100 ppmw.

## 1. Introduction

Clathrate hydrates (hereafter abbreviated as hydrates) consist of hydrogen bonded water (host) molecules forming a crystalline lattice stabilized by hydrate former (guest) molecules present in some of its cavities. These solid (ice like) compounds are stable for temperatures and pressures usually higher than the water/ice transition temperature (0 °C) and the atmospheric pressure. Since most hydrate formers are sparingly soluble in water, hydrates

usually appear and grow at/from the interface between the (liquid or gas) guest phase and the water rich phase. The formation, growth and morphology of hydrates at guest/water interfaces under quiescent conditions are the focus of increasing interest, motivated both by fundamental reasons and practical applications (Chatti et al., 2005; Sloan and Koh, 2008).

On the fundamental side, the respective roles of heat and mass transfers (Mochizuki and Mori, 2006; Saito et al., 2010; Sun et al., 2010) and of surfactant molecules added in small amounts to the water or guest phases (Zhong and Rogers, 2000; Karanjkar et al., 2012; Mitarai et al., in press) are not yet fully understood. When the hydrate former is sparingly soluble in water, hydrate formation occurs at the water/guest interface, along which a

\* Corresponding author. Tel.: +33 559407685; fax: +33 559407725.  
E-mail address: [daniel.broseta@univ-pau.fr](mailto:daniel.broseta@univ-pau.fr) (D. Broseta).

polycrystalline thin crust grows rapidly (Taylor et al., 2007). This thin crust contains gas filled pores that anneal over time, which increases resistance to mass transfer (Davies et al., 2010) and results in a very slow crust thickening and growth normal to the interface: over reasonable timescales and under quiescent conditions, much of the water trapped beneath this hydrate crust remains unconverted (Sloan and Koh, 2008). In some (rare) instances, however, the growing porous structure, rather than forming a low permeable thin crust at the guest/water interface, allows much of the water (if guest molecules are in excess) to be rapidly and totally converted into hydrate. This still ill understood hydrate formation mechanism (often referred to as ‘capillary driven’) is encountered for instance with methane and low molecular weight alkanes (but not with CO<sub>2</sub>) when anionic surfactant additives such as sodium alkyl sulfates (e.g., sodium dodecyl sulfonate or SDS) are added to the water in small amounts (typically, a few hundreds of ppm) (Zhong and Rogers 2000; Sun et al., 2003a, b; Lin et al., 2004; Gayet et al., 2005; Okutani et al., 2008).

On the side of practical applications, the ability to speed up hydrate formation and growth is key to the success of emerging hydrate based technologies such as natural gas or hydrogen storage and transportation by means of hydrates, refrigeration processes using hydrates as a phase change material, CO<sub>2</sub> separation, water purification and desalination, etc. Clearly, a capillary driven mechanism (promoted by proper surfactant additives) of hydrate formation is preferred for these applications, unless a large amount of guest/water interfaces is generated by, e.g., mechanical agitation, spraying/bubbling one phase into the other (Gnanendran and Amin, 2004; Brinchi et al., 2014), or circulating the guest phase through mesoporous particles saturated with water (Dicharry et al., 2013). In other applications such as oil and gas transport through pipelines, hydrate formation and growth must be impeded to ensure flow, which is achieved by using low dosage (a few hundreds to thousands of ppm) water soluble molecules called kinetic hydrate inhibitors (KHIs). The performance of these KHIs might be related to their ability to slow down the lateral growth of the hydrate crust at the water/guest interface where they usually adsorb (Peng et al., 2009; Duchateau et al., 2012; Wu et al., 2013); another important factor seems to be the localization of hydrate growth at the interface, which impedes or delays the growth of a 3D porous structure by the capillary driven flow mechanism mentioned above.

This paper presents an experimental investigation of hydrate growth at the interface between water and mixtures of CO<sub>2</sub> and CH<sub>4</sub> as a function of temperature, pressure, gas composition and surfactant additives present in the water phase. The following aspects are examined: hydrate crust morphologies and lateral growth rates, and capillary driven growth in the presence of some surfactant additives.

Studies on hydrate growth at the interface between the aqueous and guest phases have recently been reviewed by Sun et al. (2010), who did not however consider water/guest systems in which the guest phase is a mixture of gases and/or an aqueous phase containing a small amount of surfactant additives. We therefore first briefly review the work done on these systems, after reviewing for completeness that on pure water/CO<sub>2</sub> and /CH<sub>4</sub> systems.

Uchida et al. (1999) were the first to report observations of CO<sub>2</sub> hydrate growing on the surface of water droplet suspended in CO<sub>2</sub> and noticed that the propagation rate is primarily dependent on, and an increasing function of, subcooling  $\Delta T = T_{\text{eq}} - T_{\text{exp}}$ , where  $T_{\text{exp}}$  is the temperature of the experiment and  $T_{\text{eq}}$  the dissociation temperature (i.e., the temperature of hydrate/water/gas equilibrium) at the pressure of the experiment. A similar dependence was observed by Freer et al. (2001) for CH<sub>4</sub> hydrate growing at a water/CH<sub>4</sub> (planar) interface, albeit at a rate lower by about one order of magnitude than CO<sub>2</sub> hydrate at similar subcooling. These and other authors (Servio and Englezos, 2003; Ohmura et al., 2004) examined hydrate crust mor-

phologies: a more faceted aspect (individual crystals of millimeter sizes) is observed at low subcooling  $\Delta T$ , while a smooth appearance is noted at intermediate and high  $\Delta T$ . Extensive observations of hydrate crust texture and lateral growth at water/gas interfaces have been conducted over the past decade, most of them focused on water/CH<sub>4</sub> systems, using various configurations: a rising (gas) bubble in water (Peng et al., 2007; Sun et al., 2007; Li et al., 2013, 2014), a water drop (in gas) either pendent (Zhong et al., 2011) or sitting on a substrate (Tanaka et al., 2009), or a planar water/gas interface (Kitamura and Mori, 2013). While there is some scatter in the published lateral growth rates, all observations show that the hydrate crust texture gets smoother with increasing subcooling and increasing time. The variation of lateral growth rates with subcooling is accounted for by models in which heat transfer processes at the edge of the advancing hydrate front is the controlling factor (Mochizuki and Mori, 2006; Sun et al., 2010), but mass transfer limitations appear to play an important role as well (Saito et al., 2010).

A few studies have been conducted with gas mixtures as the guest phase or with some water soluble additives present in the water phase. The measurements by Peng et al. (2007) of hydrate growth at the surface of bubbles (in pure water) of various CH<sub>4</sub>+C<sub>2</sub>H<sub>4</sub> mixtures, as well as one CH<sub>4</sub>+C<sub>3</sub>H<sub>8</sub> mixture, indicate lateral growth rates smaller than those of the corresponding pure water/pure gas systems. A similar effect has been observed with CH<sub>4</sub>+C<sub>2</sub>H<sub>6</sub> mixtures by Li et al. (2014), who argued that the coexistence in the hydrate crust of two crystalline structures (I and II) might be responsible for the slowing down of the frontal advance. However, the latter effect was not observed in the experiments conducted by Saito et al. (2011) on sessile water drops with two CH<sub>4</sub> rich (90+ mol. %) mixtures of CH<sub>4</sub>, C<sub>2</sub>H<sub>6</sub>, and C<sub>3</sub>H<sub>8</sub>. The studies conducted with surfactant or polymeric additives present in the water phase are of two sorts. One is concerned with polymeric additives inhibiting hydrate formation (KHIs), which delay nucleation and/or slow down hydrate film lateral growth at water/guest interfaces (Peng et al., 2009; Duchateau et al., 2012; Wu et al., 2013). The other is concerned with additives (such as SDS) promoting hydrate formation. The understanding of these promoting processes, loosely referred to as ‘capillary driven’, is one of the most challenging fundamental issues in gas hydrate research, whereas on a more practical side simple and rapid methods are needed for assessing the hydrate promoting potential of a given additive. As stated by Lo et al. (2012), finding the efficient surfactant(s) among the hundreds of existing surfactants is currently like ‘finding a needle in a hay stack’: quick assessment methods such as those proposed by these authors, or the drop based method proposed in this paper, are urgently needed.

The outline is as follows: The next section describes the gases and surfactant additives used, as well as the apparatus and experimental methodology for forming and visualizing hydrate growth on/in a water drop in a gas atmosphere at controlled pressure and temperature. Then, in Section 3, the results obtained with pure water are presented and discussed: the effects of gas composition, temperature and pressure on hydrate crust texture and growth rate are analysed in detail. Section 4 is devoted to the results obtained under the same conditions as in Section 3, with the difference that a small amount of surfactant is present in the water phase: some insights are given into capillary driven hydrate formation.

## 2. Experiments

### 2.1. Materials

CO<sub>2</sub> and CH<sub>4</sub> were purchased from Linde (99.995%) and CO<sub>2</sub>/CH<sub>4</sub> mixtures from Air Liquide (see Table 1 for compositions).

**Table 1**  
Compositions of the CO<sub>2</sub>/CH<sub>4</sub> gas mixtures used in the experiments (as given by Air Liquide).

No. of mixed gas sample	CO <sub>2</sub> , mol%	CH <sub>4</sub> , mol%
1	q. s	24.98 ± 0.50
2	q. s.	49.60 ± 0.99
3	25.08 ± 0.50	q.s

Those compounds and mixtures were used in the experiments under monophasic (gas) conditions, i.e., at low enough pressures in order to avoid the condensation of the CO<sub>2</sub> rich mixtures at the temperatures of interest (from 0 to 5 °C). Water is deionized and has a resistivity of 18 MΩ cm.

## 2.2. Surfactant additives

### 2.2.1. Non ionic surfactants

The non ionic surfactants, chosen for their reported ability to lower the interfacial tension and/or to promote emulsions between water and dense (supercritical) CO<sub>2</sub>, belong to four different classes. Some of them have been already tested in the context of gas hydrate research (Sun et al., 2003a, b; Zhang et al., 2008; Zhong et al., 2008; Delahaye et al., 2011; Dicharry et al., 2013). The first class of surfactants consists of polyoxyethylene sorbitan fatty acid esters, with commercial names Tween<sup>®</sup> plus a number specifying the fatty acid: 20 (monolaurate), 40 (monopalmitate), 60 (monostearate) and 80 (monooleate). The second class consists of polyethylene oxide/propylene oxide triblock or random copolymers with commercial names Pluronic<sup>®</sup>; they are called by a letter (for the physical state: L for liquid, P for paste) and a number for the molecular weight (first one or two digits) and the proportion of ethylene oxide monomers (last digit) and in between the letter R if the copolymer is random. The third class of surfactants consists of polyethylene oxide 2,6,8 trimethyl 4 nonyl ethers known as Tergitol<sup>®</sup> TMNn, where n(=6 and 10 in the present study) is the number of ethylene oxide monomers. Lastly, an ethoxylated acetylenic diol with trade name Surfynol 465 has been tested. The characteristics (supplier, molecular weight, hydrophilic lipophilic balance or HLB) and molecular formulae of the surfactants tested are listed respectively in Table S1 and Figure S1 of [Supplementary material](#).

### 2.2.2. Anionic surfactants

The anionic surfactants tested (only with pure CH<sub>4</sub> and pure CO<sub>2</sub>) are SDS (sodium dodecyl sulfate) dissolved in water at concentrations of 100 and 500 ppmw (i.e., 0.01 and 0.05 wt%), and a common Gemini (double tailed) surfactant, dioctyl sodium sulfocinate (also known as AOT), at a concentration of 100 ppmw. SDS is chosen because this is the prototypical CH<sub>4</sub> hydrate promoter. Gemini surfactants need a lower dosage than SDS for a given surface tension decrease and activity at water/hydrate interfaces (Salako et al., 2013). Some of these surfactants have been observed to give comparable formation rates and higher methane storage capacities than SDS at very low dosage (below 150 ppm) (Kwon et al., 2011).

### 2.2.3. Interfacial behavior

The interfacial tensions between the aqueous and gas phases were measured in the course of the drop experiments (see below) at the experimental temperatures (from 0 to 5 °C) and pressures (from 27 to 40 bar); the contact angles of a drop of the aqueous solutions on PTFE, a strongly hydrophobic substrate, were measured as well (see [Section 2.3](#) for the measurement method). The above surfactants indeed lowered water/guest interfacial tensions and rendered the

substrate less hydrophobic, but in limited manner for most solutions (see Table S2 in [Supplementary material](#)). All tensions remained above 20 mN/m and contact angles (measured in the aqueous phase) above 50–60°, except for the 1000 ppmw Tergitol<sup>®</sup> TMN6 and TMN10 solutions that exhibited (see Table S2) lower tensions and angles in presence of CO<sub>2</sub> (no measurement was attempted with the other gases).

## 2.3. Experimental apparatus and procedure

The experiments of hydrate growth at the water/gas interface of a water drop are conducted under controlled temperature and pressure. Hydrate formation is triggered at the top of a sessile water drop (in a gas atmosphere) by contact with another hydrate hanging at the tip of a capillary, then the subsequent hydrate growth is monitored by means of an image acquisition and treatment system. The procedure is similar to that used by Peng et al. (2007), Sun et al. (2007) and Li et al. (2014), with the difference that these researchers nucleated the hydrate at the top a gas bubble (immersed in the aqueous phase) by contact with another gas bubble covered with hydrate.

The experimental apparatus, schematically presented in [Fig. 1](#), consists of

- A high pressure (maximum operating pressure: 20 MPa) view ing cell (volume 17 cm<sup>3</sup>) with two parallel see through sap phire windows of 18 mm diameter, designed in collaboration with Top Industrie (France). The cell contains a horizontal plate and a vertically moveable capillary tube connected to a Teledyne ISCO Syringe Pump (100 DM) allowing a drop of the aqueous phase to be formed at the tip of the capillary and eventually be deposited on the horizontal plate. The cell and plate temperatures are controlled independently by means of two refrigerating/heating circulation systems (Fischer Scientific Polystat 37). The temperature in the cell is measured by means of a Pt100 sensor with an accuracy of 0.1 °C.
- An optical and imaging system, composed of a diffuse light source, a CCD camera (Toshiba 8 bits; maximum acquisition speed: 25 fps; sensor size: 6.5 mm × 4.85 mm, 752 × 582 pixels, 680 × 480 of which are exploited in the image treat ment software) and a PC. The image treatment software (Windrop<sup>™</sup>, Teclis, Longessaigne, France) provides the contour of the sessile drop for each image and computes the drop area and volume, as well as the contact angle and int erfacial tension (the contour is analyzed in terms of the Young Laplace equation, provided phase densities are given for details see [Broseta et al., 2012](#)).

The experimental procedure comprises the following steps:

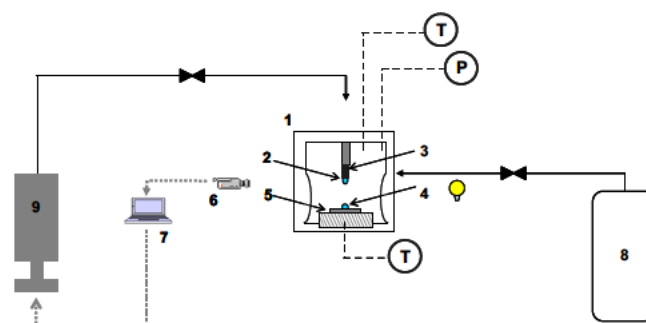


**Fig. 1.** Schematic diagram of the experimental apparatus. (1) high-pressure cell, (2) pendant drop, (3) capillary tube, (4) sessile drop, (5) temperature-controlled plate, (6) CCD camera, (7) computer, (8) gas storage vessel, (9) syringe pump.

- (1) Gas is flushed into the cell and evacuated three times in order to evacuate air.
- (2) The cell is filled with gas at the operating pressure at ambient temperature.
- (3) A drop of the aqueous phase is deposited by means of the vertically moving capillary tube on the horizontal plate previously (unless otherwise specified) covered with a PTFE film. In all measurements presented here, the area of this sessile water drop, denoted  $a$ , lies in the range of  $40 \pm 8 \text{ mm}^2$ .
- (4) The cell temperature is then lowered to  $-3 \text{ }^\circ\text{C}$  and gas is injected into the cell to compensate for the pressure decrease. Spontaneous hydrate nucleation may occur at the surface of the sessile water drop: in this case, the experiment is restarted and cell temperature is brought to, e.g.,  $-2 \text{ }^\circ\text{C}$ .
- (5) Gas hydrate (to be used for triggering hydrate formation by contact with the top of the sessile drop, see step 6) is formed at the tip of the capillary as follows: a pendant water drop formed at the tip of the capillary is first pumped into the upper part of the capillary, which is cooled down to about  $-30 \text{ }^\circ\text{C}$  by contact with the immersion probe of a Julabo FT401 immersion cooler, then the pump pushes back to the tip of the capillary some crystallized water that reacts with the ambient gas to form hydrates (Fig. 2(a)). The sessile water drop (see step 3) is still fully liquid.
- (6) Temperature is raised to the desired value, and the system left to equilibrate for a while. The hydrate crystal hanging at the tip of the capillary (see step 5) is then brought in contact with the top of liquid sessile drop by moving the capillary downwards (Fig. 2(b)), which triggers hydrate formation and subsequent growth. In most situations, hydrate growth consists in the propagation of a hydrate crust at the surface of the sessile water drop starting from the contact point to the base of the sessile water drop. This process is recorded with the CCD camera until there is no detectable change or movement. One of the recorded movies (corresponding to the snapshots of

Fig. 2) is available in the supplementary information (movie M1). Two types of information are extracted from these movies:

Supplementary material related to this article can be found online at <http://dx.doi.org/10.1016/j.ces.2015.04.015>.

The morphology (or texture) of the gas hydrate crust formed at the interface between water and gas and its evolution with time, the growth rate of the hydrate crust, defined as an average surface (or two dimensional) rate  $r_a$  equal to the sessile drop area  $a$  divided by the time  $t_f$  required for the drop to appear as 'frozen' or immobile (see Appendix A) or as an average linear rate  $r_l$ , equal to the drop contour divided by  $2 \times t_f$  (the hydrate crust travels from the top to the base of the drop); following Sun et al. (2007), surface rates  $r_a$  are reported here, and linear rates are evaluated only with pure  $\text{CO}_2$  and pure  $\text{CH}_4$  for the purpose of comparison with published results.

The plate is heated for several minutes in order to dissociate the hydrate on the sessile water drop, while the cell remains at the operating temperature; some crystallized gas hydrate remains hanging at the tip of the capillary previously raised to the upper part of the cell (see Step 6).

Then, a new measurement is started by bringing the crystallized gas hydrate in contact with the sessile water drop (step 6, etc).

A minimum of four measurements is carried out for each temperature, pressure, gas and aqueous phase composition, from which the average growth rate is calculated, together with the related standard deviation. The results are reported in Table 2 (pure water) and S2 in Supplementary material.

The independent temperature control of the plate is very practical for carrying out numerous consecutive runs and for assessing the reproducibility of growth rate measurements. No gas consumption is detected during experiments due to the very small volume of hydrate formed by comparison with the cell volume. The features of the CCD

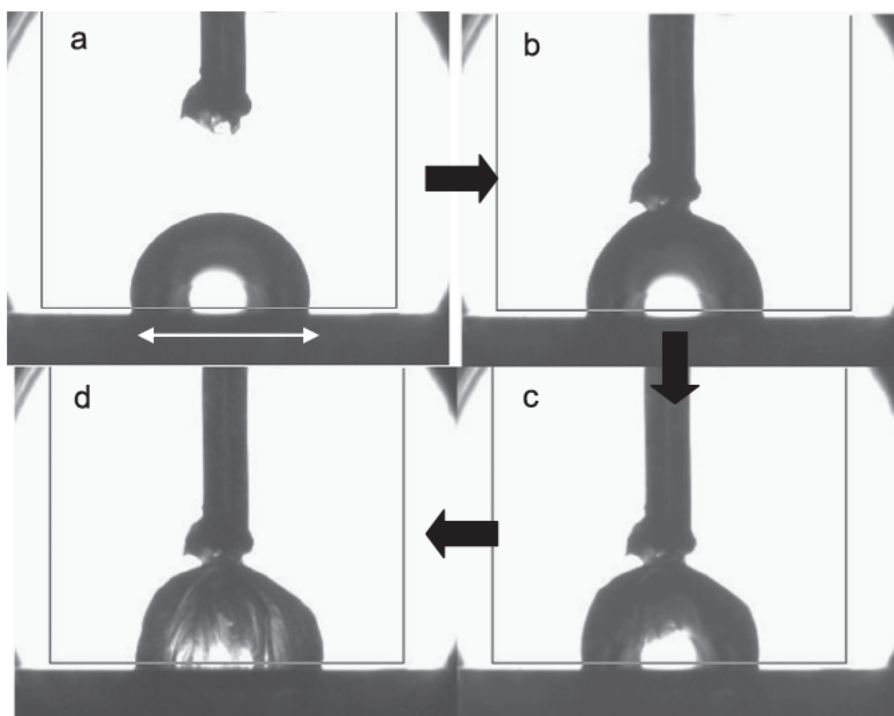


Fig. 2. Snapshots of  $\text{CO}_2$ -hydrate growth on a sessile water drop (at 26.6 bar,  $5 \text{ }^\circ\text{C}$ ) showing the approach of the capillary with a hydrate phase at its extremity (a), contact of this hydrate with the top of the water drop (b), propagation of the hydrate crust along the surface of the drop (c) and final aspect of the drop (d). Duration of crust propagation is about 15 s. Drop diameter (white arrow) is equal to 4.5 mm. (See movie M1, Supplementary material.)

**Table 2**

Experimental conditions and results of hydrate lateral growth rate measurements on a pure water drop for pure gases (CO<sub>2</sub>, CH<sub>4</sub>) and the three CO<sub>2</sub>/CH<sub>4</sub> mixtures with compositions given in Table 1. The three-phase (hydrate/water/gas) equilibria pressures  $P_{eq}$  at the experimental temperatures  $T_{exp}$  are calculated by using the CSMGem software.  $-\Delta g/RT$  is the dimensionless driving force, which is defined in Appendix B.

	$P_{exp}$ , bar	$T_{exp}$ , °C	$P_{eq}$ , bar	$\Delta T$ , °C	$T_{eq}-T_{exp}$	$-\Delta g/RT$	$r_a$ mm <sup>2</sup> s <sup>-1</sup>	$r_l$ mm s <sup>-1</sup>	
Pure CO <sub>2</sub>	26.6	5.0	22.5	1.18		0.168	3.1 ± 0.8	2.0 ± 0.25	
	26.7	3.5	18.85	2.75		0.348	10.7 ± 1.0	7.25 ± 1.9	
	26.45	2	15.6	4.16		0.528	22.1 ± 5.1	20.5 ± 2.1	
	27	2	15.6	4.32		0.548	24.7 <sup>(a)</sup>		
	27	0	12.0	6.27		0.811	48.1 <sup>(a)</sup>		
	27.4	3.5	20.4	2.48		0.300	3.1 ± 0.4		
75% CO <sub>2</sub>	30.4	3.5	20.4	3.32		0.406	7.4 ± 0.6		
25% CH <sub>4</sub>	27.2	2	17.12	3.92		0.468	8.3 ± 0.7		
	30.3	0	13.62	4.79		0.578	15.9 ± 1.0		
	27.1	0	13.62	5.89		0.6953	17.1 ± 4.9		
	30	0	13.62	6.70		0.799	27.4 ± 3.4		
	30	3.5	23.25	2.23		0.257	0.77 <sup>(b)</sup>		
50% CO <sub>2</sub>	27	2	19.65	2.93		0.320	1.3 <sup>(b)</sup>		
50% CH <sub>4</sub>	35	4	24.6	3.04		0.355	1.2 ± 0.3		
	40	5	27.6	3.14		0.375	1.2 ± 0.3		
	30	2	19.65	3.73		0.426	2.4 ± 0.3		
	27	1	17.6	3.93		0.430	2.25 <sup>(b)</sup>		
	35	3	22.0	4.04		0.469	1.9 ± 0.2		
	30	1	17.6	4.73		0.537	3.9 ± 0.3		
	27	0	15.75	4.93		0.542	3.7 ± 0.9		
	35	2	19.65	5.04		0.582	4.5 ± 0.5		
	40	3	22.0	5.14		0.604	3.5 ± 0.3		
	30	0	15.75	5.73		0.648	6.3 ± 0.9		
	35	1	17.6	6.04		0.692	7.4 ± 0.4		
	35	2	23.55	3.65		0.386	2.7 ± 0.4		
	25% CO <sub>2</sub>	30	0	19.05	4.24		0.445	2.7 ± 0.5	
	75% CH <sub>4</sub>	40	2	23.55	4.85		0.516	3.4 ± 0.3	
40		1	21.2	5.85		0.620	5.2 ± 0.5		
45		2	23.55	5.98		0.630	5.6 ± 0.7		
45		1	21.2	6.89		0.734	7.1 ± 0.3		
45		0	19.05	7.89		0.838	10.2 ± 1.7		
Pure CH <sub>4</sub>	40	0	26.3	4.31		0.374	1.6 ± 0.2	0.15 ± 0.03	
	45	1	28.3	4.47		0.405	1.8 ± 0.2	0.22 ± 0.02	
	45	0	26.0	5.47		0.477	2.7 ± 0.4	0.32 ± 0.02	

<sup>a</sup> Spontaneous nucleation occurred prior to hydrate contact in most experiments.

<sup>b</sup> Standard deviation not indicated: less than 4 measurements done.

camera limit the range of pressures and temperatures investigated: for high driving forces (i.e., high pressure and low temperatures), growth is too rapid to be detected by the CCD camera.

### 3. Results and discussion: experiments conducted with pure water

The drop experiments carried out with pure water, CO<sub>2</sub>, CH<sub>4</sub> and various CO<sub>2</sub>/CH<sub>4</sub> gas mixtures (with compositions given in Table 1) are presented first. They have been conducted at temperatures  $T_{exp}$  in the range of 0–5 °C and pressures  $P_{exp}$  not exceeding 45 bar in the case of pure CH<sub>4</sub> and 27 bar in the case of pure CO<sub>2</sub> (and intermediate values for the gas mixtures), in such a way that the non-aqueous phase remains gaseous. Unless otherwise specified, each line in Table 2 corresponds to a set of (at least four) experiments conducted with the same gas composition, pressure and temperature conditions (columns 1–3). The subcooling  $\Delta T = T_{eq} - T_{exp}$ , where  $T_{eq}$  is the dissociation temperature at  $P_{exp}$  ( $T_{eq}$  is determined by using the software CSMGem, Sloan and Koh, 2008) and the dimensionless driving force (see Appendix B) are reported in columns 4 and 5. (For the conditions investigated here, the dimensionless driving force is proportional to the subcooling  $\Delta T$ , in agreement with previous results on similar

systems, see Arjmandi et al., 2005). Finally, the average of the measured growth rates  $r_a$  and the associated standard deviations are reported in the rightmost column of Table 2, together with the linear rates  $r_l$  (in the case of pure CO<sub>2</sub> and pure CH<sub>4</sub> only).

In the case of pure CH<sub>4</sub>, the hydrate crusts formed on the water drop surface are barely visible (they are smoother and thinner, see next section): the results corresponding to only three different temperature and pressure conditions are reported in Table 2.

The results displayed in Table 2 clearly indicate that the growth of the hydrate crust is more rapid at higher subcooling  $\Delta T$  and higher CO<sub>2</sub> content in the guest gas. Morphological aspects are examined prior to presenting and discussing growth rates in a quantitative fashion.

#### 3.1. Hydrate morphologies

The morphology (or texture) of the hydrate crust covering the water drop is observed to vary with gas composition and driving force (or subcooling). This morphology experiences some changes after the drop has been fully covered with hydrate, as commented below.

#### 3.2. Effect of gas composition and driving force (or subcooling)

Fig. 3 depicts the final aspect of a water drop covered with hydrate crusts formed at similar subcooling (3–4 °C) but different compositions ranging from 100% to 0% CO<sub>2</sub>. Hydrate layers of pure methane (and methane rich) hydrates are smooth and their presence at the drop surface barely alters the shape of the initial water drop, whereas CO<sub>2</sub> hydrate crusts show well defined crystalline facets with significant changes in surface curvatures compared to the initial water drop (see Fig. 2). As to the effect of subcooling, the hydrate crusts are smoother when the driving force increases, as illustrated in the case of CO<sub>2</sub> in Fig. 4.

These observations are worth being compared with those reported in the literature, particularly those by Peng et al. (2007) and Sun et al. (2007). These authors observed CO<sub>2</sub> hydrate crusts rougher (and thicker) than CH<sub>4</sub> hydrate crusts (see Figure 14 in Peng et al., 2007) and smoother hydrate crusts for higher driving forces (see Fig. 9 in Sun et al., 2007). The high resolution optical studies recently conducted by Tanaka et al. (2009), Kitamura and Mori (2013) and Li et al. (2014) show that, at high driving force ( $\Delta T > 3$ –4 K), the polycrystalline crust is made up of very tiny crystals (in the micron range) and thus looks smooth under moderate magnification, whereas at low driving force (below  $\Delta T = 1$  K in the case of CH<sub>4</sub> hydrates) the crystallites grow to large (a few tens to hundreds of  $\mu\text{m}$ ) faceted or polygonal shapes.

In many experiments, changes are still occurring after the water drop has been fully covered with hydrate. In some instances, a second hydrate layer seems to follow the formation of the first hydrate crust, resulting in a smoother surface, or in the smoothening of an initially textured crust: see Fig. 5 that depicts how the hydrate crust formed from pure water and a 25 mol% CO<sub>2</sub>/75 mol% CH<sub>4</sub> gas mixture has its vertical stripes smoothed out within about one second (this smoothening proceeds from the top to the bottom of the drop in such a way that it looks like a second hydrate crust is propagating). A possible mechanism is as follows: the thinner regions of the initially irregular crust are more permeable to gas and water and therefore get thicker more rapidly. This phenomenon has been observed by Uchida et al. (1999) at the interface between water and CO<sub>2</sub>, and by Zhong et al. (2011) at the interface between water and CH<sub>4</sub>.

#### 3.3. Lateral growth rates

The measured lateral growth rates  $r_a$  given in Table 2 are displayed as a function of subcooling  $\Delta T$  in Fig. 6 for the pure CH<sub>4</sub> and CO<sub>2</sub> and the three CH<sub>4</sub>/CO<sub>2</sub> mixtures investigated. For a given

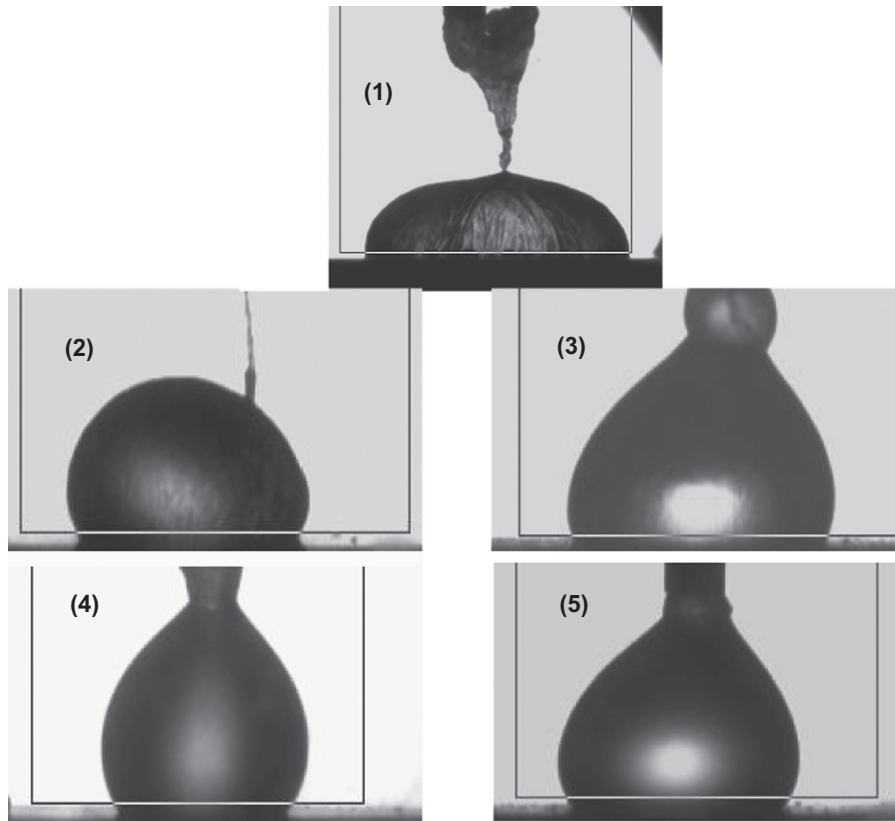


**Fig. 3.** Influence of guest gas composition on hydrate crust morphology ( $\Delta T = 3 \pm 0.5$  °C): (1) pure CO<sub>2</sub>, (2) CO<sub>2</sub>/CH<sub>4</sub>, 75/25 mol%, (3) CO<sub>2</sub>/CH<sub>4</sub>, 50/50 mol%, (4) CO<sub>2</sub>/CH<sub>4</sub>, 25/75 mol%, and (5) pure CH<sub>4</sub>.

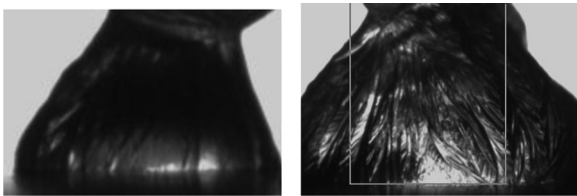


**Fig. 4.** CO<sub>2</sub>-hydrate crystal on a water drop at 27 bar and 2 °C (left) and 5 °C (right).

guest gas, these rates strongly increase with subcooling as a power of  $\Delta T$  with an exponent in the range of 2 (see Fig. 6) in agreement with many observations (Peng et al., 2007; Sun et al., 2007) and with a theoretical approach based on heat transfer considerations (that predicts an exponent equal to 2.5, see Mochizuki and Mori, 2006; Peng et al., 2007). A good fit of the data is also provided by the exponential correlation proposed by Sun et al. (2007),  $r_a = A[\exp(-B\Delta g/RT) - 1]$ , where  $\Delta g/RT$  is the dimensionless driving force (see Appendix B). For a given subcooling  $\Delta T$ , growth rates strongly increase with the fraction of CO<sub>2</sub> in the guest gas. For example, at  $\Delta T \approx 5.5$  °C, growth rates increase by more than one order of magnitude, from  $2.7 \text{ mm}^2 \text{ s}^{-1}$  (pure methane) to nearly  $40 \text{ mm}^2 \text{ s}^{-1}$  (pure CO<sub>2</sub>). This increase is strongly non linear: it is moderate (less than a 2 fold increase) when the CO<sub>2</sub> molar content increases from 0% (pure CH<sub>4</sub>) to 25% and to 50%, and more pronounced when the CO<sub>2</sub> content increases from 50% to 75% and to 100% (see Fig. 6).

Our three data points on CH<sub>4</sub> hydrate growth rates can straightforwardly be compared to those of Sun et al. (2007), who observed for dimensionless driving forces from 0.37 to 0.48 growth rates increasing from  $1.0$  to  $1.7 \text{ mm}^2 \text{ s}^{-1}$ , slightly lower than our values from  $1.4$  to  $2.7 \text{ mm}^2 \text{ s}^{-1}$ . This difference might be ascribed to the different

configuration and procedures: a quicker removal of the heat generated by hydrate formation is ensured in our experiments, where the configuration is that of a sessile water drop in a gas environment, whereas that of Sun et al. (2007) is that of a gas bubble immersed in water; in addition, the sessile water drop is placed onto a cooled plate in our procedure, whereas only the cell as a whole is temperature controlled in the experiments by Sun et al. (2007).

The measured linear rates  $r_l$  (rightmost column in Table 2) are in line with those observed with CO<sub>2</sub> on water drops by Uchida et al. (1999), but somewhat higher than those observed (again with CO<sub>2</sub>) by Peng et al. (2007) on gas bubbles. With CH<sub>4</sub> our results are in line with those observed by Peng et al. (2007) and by Li et al. (2014) on gas bubbles, and by Freer et al. (2001) on planar water/gas interfaces, but about twice higher than those observed by Kitamura and Mori (2013), also on planar water/gas interfaces.

To explain the observed large difference in lateral growth rates for hydrates formed from CO<sub>2</sub> (and CO<sub>2</sub> rich) gases and from CH<sub>4</sub> (and CH<sub>4</sub> rich) gases, other effects than heat transfer processes have to be taken into account, as thermal properties of these two systems are very similar. Gas solubility in water evidently plays an important role. Ohmura et al. (2004) were the first to build a model in which gas solubility (or, more precisely, the gas solubility difference between the hydrate free and hydrate containing water) controls the kinetics of hydrate growth, and later established a correlation between lateral growth rate and gas solubility (Saito et al., 2010). The monotonic trend with gas composition that we observe differs from the trend observed by Peng et al. (2007) with mixed CH<sub>4</sub>/C<sub>2</sub>H<sub>6</sub> gases and by Li et al. (2014) with mixed CH<sub>4</sub>/C<sub>2</sub>H<sub>6</sub> gases, who noted lower rates for hydrates formed from gas mixtures in comparison to the rates of the corresponding pure gas hydrates. As mentioned in the Introduction, Li et al. (2014) attributed this trend to the formation of hydrates of a different structure (II) for some mixed CH<sub>4</sub>/C<sub>2</sub>H<sub>6</sub> gases.

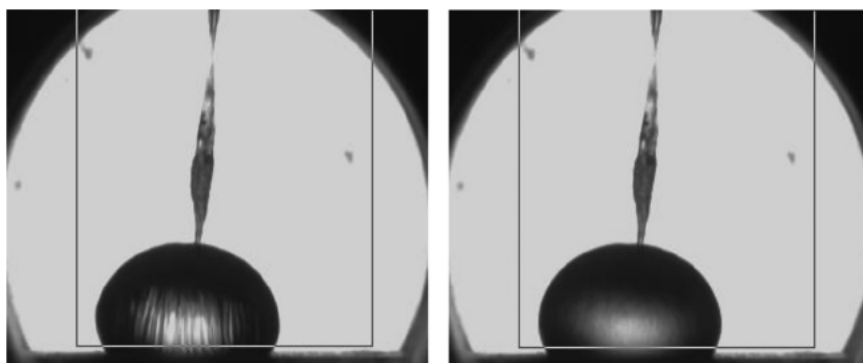


Fig. 5. Snapshots of a water drop covered with hydrate, taken about 1 s apart. Guest gas: 25 mol% CO<sub>2</sub>/ 75 mol% CH<sub>4</sub>, T = 0 °C, P = 30 bar.

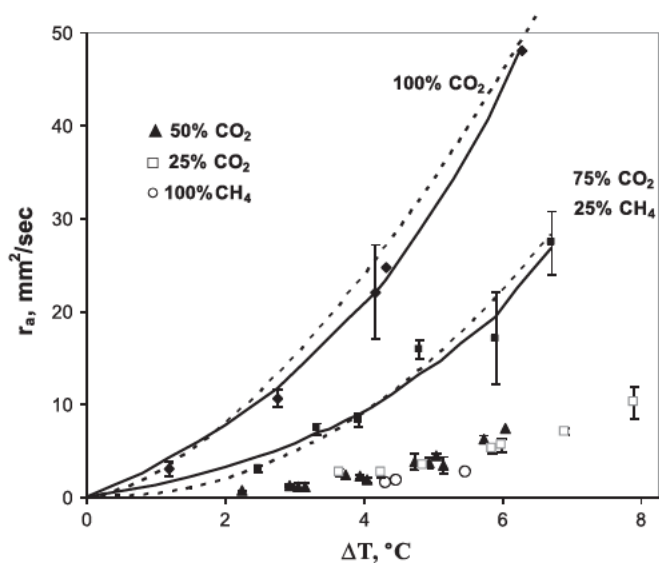


Fig. 6. Hydrate crust lateral growth rates as a function of subcooling  $\Delta T$  for various guest gases: pure (100%) CO<sub>2</sub>, 75 mol% CO<sub>2</sub>/25 mol% CH<sub>4</sub>, 50 mol% CO<sub>2</sub> and CH<sub>4</sub> (black triangles), 25 mol% CO<sub>2</sub>/75 mol% CH<sub>4</sub> (white squares) and pure (100%) CH<sub>4</sub> (black circles). The dotted curves are power-law fits with exponents 1.6 (pure CO<sub>2</sub>) and 2.2 (75% CO<sub>2</sub>). The full curves are exponential fits,  $r_a = A[\exp(-B\Delta g/RT) - 1]$ , where the driving force  $-\Delta g/RT$  is proportional to  $\Delta T$ ,  $A$  is equal to 10.9 (pure CO<sub>2</sub>) and 3.5 (75% CO<sub>2</sub>), and  $B = 2.1$  (pure CO<sub>2</sub>) and 2.7 (75% CO<sub>2</sub>).

#### 4. Results and discussion: experiments conducted with water-soluble additives

We present in this section the results of the experiments conducted with systems and conditions similar to those described in the previous section: the only difference is the composition of the aqueous phase, to which is added a small concentration (in the range of 100–1000 ppm) of non ionic or anionic surfactant molecules.

##### 4.1. Non ionic surfactants

At least one surfactant of each of the four classes of non ionic surfactants (Tweens<sup>®</sup>, Pluronics<sup>®</sup>, Tergitols<sup>®</sup> and Surfynols<sup>®</sup>, see Section 2) has been tested with the pure gases CO<sub>2</sub> and CH<sub>4</sub> and the three CO<sub>2</sub>/CH<sub>4</sub> mixtures listed in Table 1, the largest number of surfactants being tested with pure CO<sub>2</sub>. Surfactant concentration is equal to 100 ppmw in most experiments, and to 500 or 1000 ppmw in a few cases. For a given gas composition, the temperatures and pressures conditions are similar to those used with pure water (see preceding section).

All experiments conducted with a non ionic surfactant as water soluble additive do exhibit the standard growth pattern that is obs

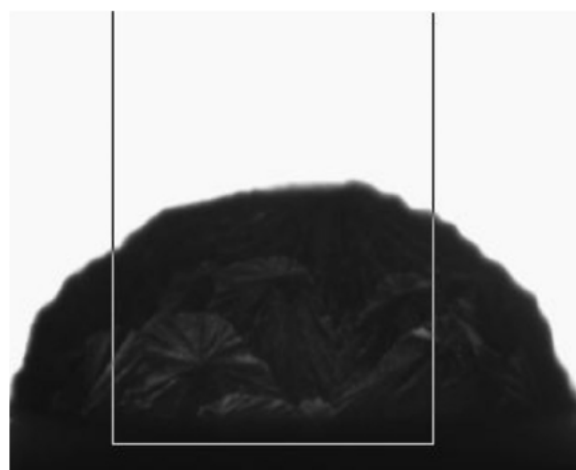


Fig. 7. Spherulites at the surface of a drop of a 1000 ppmw Pluronics P104 solution covered with CO<sub>2</sub> hydrate at 2 °C and 27 bar.

erved in the absence of additives, that is, rapid lateral growth of a hydrate crust at the interface between the aqueous and the gas phases, and growth rates are not very different from those observed in the absence of additive (see preceding section): rate values are reported in Table S2 (Supplementary material). However, morphologies may differ from one additive to the other: an example is given in Fig. 7, where spherulite like structures are apparent at the surface of a water drop containing 1000 ppmw of Pluronics (P104).

##### 4.2. Anionic surfactants: SDS and AOT

With pure CO<sub>2</sub> those two surfactants (with concentration in water equal to 100 ppmw) have little effect on hydrate growth on the drop surface, which again obeys the ‘standard’ growth pattern and exhibits rate values similar to those observed in the absence of additives (see Table S2).

With pure CH<sub>4</sub>, however, the observed hydrate growth pattern depends on both the nature of the anionic surfactant and its concentration. For the lowest SDS concentration investigated (100 ppmw) at 0 °C and 40 bar, the ‘standard’ hydrate growth pattern is observed, with a lateral growth rate somewhat higher than with pure water: 1.4 vs. 2.4 mm<sup>2</sup> s<sup>-1</sup> (Table S2). For the highest SDS concentration investigated (500 ppm) at the same T (=0 °C) and P (=40 bar), ‘capillary driven’ growth is observed: following contact at its top with the hanging hydrate (formed from a 500 ppmw SDS solution), the sessile drop is rapidly ‘swallowed’ by the hanging hydrate, which grows in size as it incorporates more water (Fig. 8 and movie M2 in Supplementary material). In this growth process all the water contained in the sessile drop is transformed into a solid hydrate phase (the gas phase being in large excess): the rightmost picture in Fig. 8,



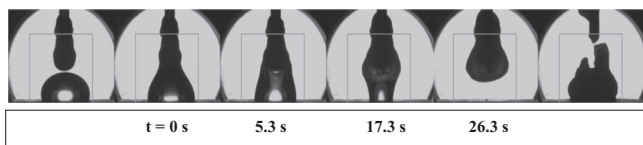


**Fig. 8.** Snapshots of CH<sub>4</sub>-hydrate growth at 0 °C and 40 bar (extracted from movie M2 of Supplementary material): the sessile drop is a 500 ppmw SDS aqueous solution, while the hanging 'drop' is the hydrate phase made from the same aqueous solution. The leftmost image is taken just before contact of the sessile drop with the hanging hydrate, which occurs at  $t = 0$ . The aqueous solution of the sessile drop rises by capillarity into the hanging hydrate phase where it is converted into hydrate. The rightmost image has been obtained after bringing the resulting hanging hydrate into contact with the substrate and then rising it until it breaks into two pieces, revealing its internal solid-like structure.

where the hanging hydrate has been broken in two pieces by contact with the lower substrate, reveals the internal solid like structure (see also movie M2 in Supplementary material).

Supplementary material related to this article can be found online at <http://dx.doi.org/10.1016/j.ces.2015.04.015>.

For the 100 ppmw AOT solution, a growth behavior is observed that is close to that observed with the 500 ppmw SDS solution, even though it proceeds more slowly and ends up in a somewhat different morphology: most of the sessile aqueous drop is 'swallowed' into the hanging hydrate (also formed from a 100 ppmw AOT solution), which undergoes a gradual and slow (within 5–6 min) transformation into a grape like structure (Fig. 9).

A strong initial wetting of the hanging CH<sub>4</sub> hydrate by the aqueous phase is apparent in the experiments involving SDS and AOT. This is particularly apparent when the hanging hydrate hits the sessile drop of aqueous solution, which immediately imbibes what looks like a porous solid like structure (see Movie M2, Supplementary material). The analogous experiments conducted with CO<sub>2</sub> do not exhibit such a strong apparent initial wetting (of the hanging CO<sub>2</sub> hydrate by the aqueous SDS or AOT solution).

The capillary driven character of gas hydrate formation is usually characterized from macroscopic measurements, e.g., from pressure or temperature variations in large volume cells, but less often from observations of the evolution of the water/gas interface over mesoscopic (sub millimetric) scales. Our results for the 100 ppmw SDS solution agree with those of Sun et al. (2007), who did notice an accelerated lateral growth of the hydrate crust along the surface of CH<sub>4</sub> bubbles in such a solution, but our results for the 500 ppmw SDS solution disagree with those by the same authors, who were able to measure lateral growth rates at the surface of CH<sub>4</sub> bubbles in a 500 ppmw SDS solution. They also differ from the recent observations by Lee et al. (2014) on bubbles of a 90/10 mol% CH<sub>4</sub>/C<sub>3</sub>H<sub>8</sub> gas mixture in very low concentrated (from 10 to 50 ppm) SDS solutions; these authors observed halos (of small hydrate crystals?) erupting and rising above the immersed gas bubble, which however preserved its integrity. Our results of the Gemini AOT surfactant (compared to that of SDS) as regards CH<sub>4</sub> hydrate formation complement those by Kwon et al. (2011) and by Salako et al., 2013, who point to a superior performance of Gemini surfactants.

One question that arises from the above observations is the following. Why is a 'capillary driven' hydrate formation process, i.e., a complete and rapid conversion of low concentrated SDS and AOT aqueous solutions into hydrate, occurring with CH<sub>4</sub> and not with CO<sub>2</sub>? This question raised by many authors (starting with Zhang and Lee, 2009) has not received any clearcut answer yet. Some molecularly based mechanisms have recently been invoked (Albertí et al., 2013), but it is likely that larger scale (mesoscopic) mechanisms are (also) at play. First insights into these mesoscale mechanisms are gained by noting the analogy between hydrate crusts growing at the aqueous surface and the salt efflorescences that grow at the evaporative surface of a porous medium saturated with brine. These efflorescences evolve between two limiting patterns, called crusty and patchy

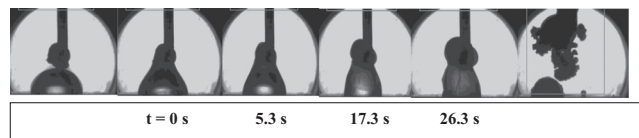


**Fig. 9.** Snapshots of CH<sub>4</sub>-hydrate growth at 0 °C and 40 bar from a 100 ppmw AOT solution. The procedure is the same as that explained in the caption of Fig. 8. The rightmost image has been obtained at about  $t = 5$  minutes, after the capillary has been raised.

by Veran Tissoires and Prat (2014), corresponding to the growth of, respectively: (i) a low permeable porous crust (of crystallized salt) that hinders further brine transport, and (ii) a highly permeable porous structure allowing brine to be continuously pumped to the top (where it evaporates and generates some further salt crystallization). The (analog of the) former pattern is what we observe here in most situations, i.e., for hydrates formed quiescently at the surface of pure water or of aqueous solutions of non ionic surfactants. The (analog of the) latter pattern, which is favored for larger pores and lower evaporation rates, i.e., slower crystallization rates (Veran Tissoires and Prat, 2014), is the capillary driven hydrate formation process: on the one hand, CH<sub>4</sub> hydrates crystallize at a lower rate than CO<sub>2</sub> hydrates (see Table 2 and Fig. 6) and, on the other hand, the porous structure (e.g., pore sizes) and wettability of the growing hydrate skeleton are likely to be influenced by the adsorption behavior of the anionic surfactant (in the case of SDS, the anionic moiety, i.e., DS<sup>-</sup>, adsorbs onto CH<sub>4</sub> hydrates but not or to a much lesser extent onto CO<sub>2</sub> hydrates, as argued by Zhang et al. (2010). Work to understand the phenomenon of capillary driven hydrate formation along these lines is in progress.

## 5. Summary and conclusions

A simple experimental method has been devised that allows a rapid assessment of the potential of a given water soluble surfactant additive in promoting hydrate growth. This method consists in triggering hydrate formation and growth at the top of a sessile water drop by contact with the hydrate phase, and in visualizing the ensuing hydrate growth. When the method is implemented with gases consisting of CH<sub>4</sub>, CO<sub>2</sub> and their mixtures, and water, either pure or containing a low concentration of a non ionic or anionic surfactant, two very different hydrate growth patterns are observed. The most prevalent growth pattern, which occurs in all situations involving pure water or a low concentrated solution of non ionic surfactant, consists in the rapid growth of a low permeable hydrate crust laterally at the water/guest interface, at a rate that increases with subcooling and CO<sub>2</sub> content, and depends much less on the nature of the non ionic surfactant, at least in the ranges of low concentrations (100 ppmw, occasionally 500 and 1000 ppmw) and low pressures not exceeding 27 bar for CO<sub>2</sub>, 45 bar for CH<sub>4</sub>, and intermediate pressures for CO<sub>2</sub>/CH<sub>4</sub> mixtures investigated. Once these interfaces are fully covered with the hydrate crust, the conversion of water and gas into hydrates is almost stopped. The other, 'capillary driven' growth pattern, is observed with methane and anionic surfactants (SDS, AOT) at concentrations in the range of 500 w and 100 ppmw, respectively: a permeable hydrate skeleton forms that continuously 'pumps' the aqueous solution and brings it in contact with the hydrate former (methane) until no water is left for conversion.

## Acknowledgments

The authors are grateful to Yahia Swedan for his help in the treatment of some of the data. This work has been supported by

### Appendix A. Image treatment procedure for determining the water drop coverage time $t_f$

This procedure exploits the following feature: after being covered with hydrate, the water drop appears to be 'frozen', i.e., it no longer moves (at least over the time scale of the experiment, i.e., at most a few minutes). This occurs at a time  $t_f$  after the drop has been contacted with hydrate at its top. This time, which is well defined because the change to a 'frozen' state occurs abruptly, is determined from an automated procedure that first splits the movie into its consecutive images (labeled by integer indexes  $i$ , each image corresponding to a specified time) and then in analyzing all sets of two consecutive images, starting from the image of first contact between the water drop and the hydrate hanging at the tip of the capillary. Each image contains  $320 \times 256$  pixels where each pixel has values from 0 (white) to 255 (black). For each couple of consecutive images (labeled by index  $i$  corresponding to the first of the two images), the following quantities are calculated:

- (i) The standard deviation of the difference between the two images,
- (ii) the correlation coefficient (corr2 in the Matlab™ library) between the two images, equal to 1 for identical images (hence, one minus this coefficient is the quantity considered), and
- (iii) the maximum pixel absolute value (on a 0-255 scale) of the difference between the two images.

An example of how those three quantities vary with  $i$  (or, equivalently, with elapsed time, as there is an interval of  $\sim 0.15$  s between two consecutive images) is shown in Figure A1, which corresponds to the experiment giving the snapshots in Fig. 2 (pure water and CO<sub>2</sub> at 5 °C and 26.6 bar).

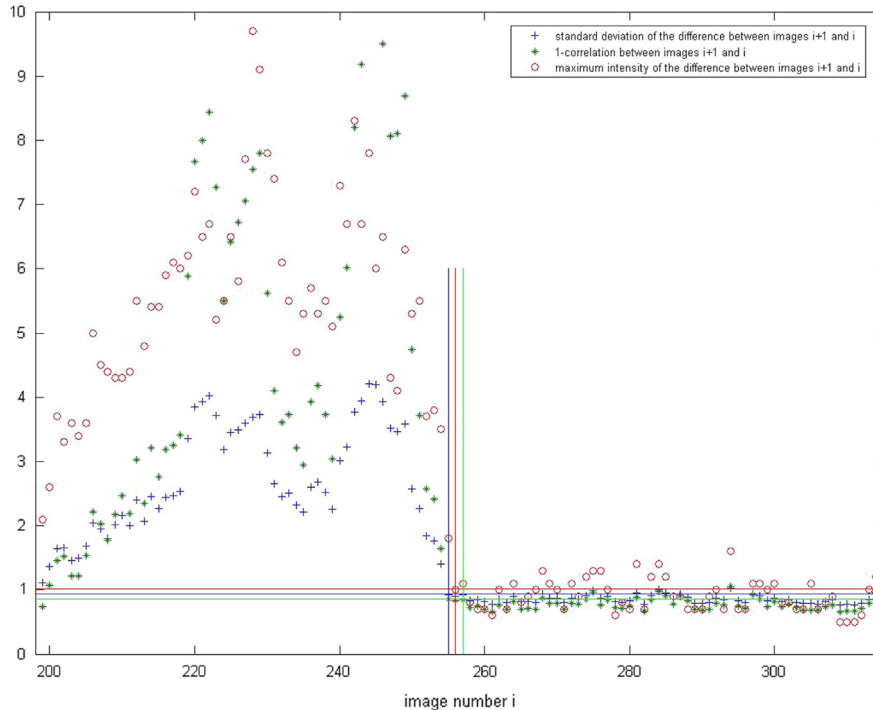


**Fig. A1.** Values of the quantities (i), (ii) and (iii) for each set of two consecutive images as a function of time or image number  $i$  (see text). The experiment is that illustrated in Fig. 2. The scale on the vertical axis is arbitrary.

We observed that, as a rule, the transition between the high values (corresponding to an advancing hydrate film) and the low values due to noise (the fully hydrate covered drop no longer moves) is very sharp and occurs at similar image number (or elapsed time) for the three above quantities, which thus provides an unambiguous determination of  $t_f$ . The corresponding image number is determined automatically in the procedure as follows.

First, the asymptotic (i.e., at large time or large index  $i$ ) average values and standard deviations of those three quantities are computed over a common range of image indexes (or elapsed time) such that these values appear fairly constant (e.g., from 260 to the maximum image number in the example of Figure A1). The quantity (iii) is prone to larger fluctuations (because it singles out one pixel) than quantities (i) and (ii): this is taken into account in the criterion for deciding when the drop starts being 'frozen' through the standard deviation, see below.

Second, the image number is decreased incrementally starting from the largest index  $i$ , and the above three quantities (i, ii, and iii) are calculated for each corresponding couple of images. When the quantity  $i$ ,  $ii$  or  $iii$  exceeds for at least three consecutive indexes its asymptotic value plus one standard deviation it is denoted by a vertical line in Figure A1. The indexes of these vertical lines usually coincide or differ very slightly, which permits times  $t_f$  to be defined unambiguously, as illustrated in Figure A1.

Third, the image number is decreased incrementally starting from the largest index  $i$ , and the above three quantities (i, ii, and iii) are calculated for each corresponding couple of images. When the quantity  $i$ ,  $ii$  or  $iii$  exceeds for at least three consecutive indexes its asymptotic value plus one standard deviation it is denoted by a vertical line in Figure A1. The indexes of these vertical lines usually coincide or differ very slightly, which permits times  $t_f$  to be defined unambiguously, as illustrated in Figure A1.

### Appendix B. Calculation of the dimensionless driving force

The driving force at a certain temperature  $T$  and pressure  $P$  below the equilibrium pressure  $P^{eq}$  is defined as  $\Delta g$ , the molar Gibbs free energy difference between the experimental and equilibrium conditions (the minus sign is to render the expression positive):

$$\Delta g = v_w (P^{eq} - P) + RT \sum x_i \ln \left( \frac{f_i^{eq}}{f_i^{exp}} \right)$$

$$+v_h(P - P^{eq}) = RT \sum x_i \ln \left( \frac{f_i^{eq}}{f_i^{exp}} \right) + \Delta v(P - P^{eq}),$$

where  $f_i^{exp}$  and  $f_i^{eq}$  are the fugacities of component  $i$  (CO<sub>2</sub> and CH<sub>4</sub>) at experimental and equilibrium conditions, and  $x_i$  is the mole fraction of component  $i$  in the gas phase, respectively; they are calculated by the Peng–Robinson equation of state.  $v_w$  is the molar volume of liquid water,  $v_h$  is the molar volume of water in hydrate and  $\Delta v = v_h - v_w$ . The dimensionless driving force is the driving force divided by  $RT$ , where  $R=8.3145$  J/molK is the perfect gas constant.#

## Appendix C. Supplementary data

Supplementary data associated with this article can be found in the online version at <http://dx.doi.org/10.1016/j.ces.2015.04.015>.

## References

- Alberti, M., Pirani, F., Laganà, A., 2013. Carbon dioxide clathrate hydrates: selective role of intermolecular interactions and action of the SDS catalyst. *J. Phys. Chem. A* 117, 6991–7000.
- Arjmandi, M., Tohidi, B., Danesh, A., Todd, A.C., 2005. Is subcooling the right driving force for testing low dosage inhibitors? *Chem. Eng. Sci.* 60, 1212–1224.
- Brinchi, L., Castellani, B., Rossia, F., Cotana, F., Morini, E., Nicolini, A., Filipponi, A., 2014. Experimental investigations on scaled-up methane hydrate production with surfactant promotion: energy considerations. *J. Pet. Eng. Sci.* 120, 187–193.
- Broseta, D., Tonnet, N., Shah, V., 2012. Are rocks still water-wet in the presence of dense CO<sub>2</sub> or H<sub>2</sub>S? *Geofluids* 12, 280–294.
- Chatti, I., Delahaye, A., Fournaison, L., Petit, J.P., 2005. Benefits and drawbacks of clathrate hydrates: a review of their areas of interest. *Energy Convers. Manag.* 46, 1333–1343.
- Davies, S.R., Sloan, E.D., Sum, A.K., Koh, C.A., 2010. In situ studies of the mass transfer mechanism across a methane hydrate film using high-resolution confocal Raman spectroscopy. *J. Phys. Chem. C* 114, 1173–1180.
- Delahaye, A., Fournaison, L., Jerbi, S., Mayoufi, N., 2011. Rheological properties of CO<sub>2</sub> hydrate slurry flow in presence of additives. *I&EC Research* 50, 8344–8353.
- Dicharry, C., Duchateau, C., Asbai, H., Broseta, D., Torré, J.P., 2013. Carbon dioxide gas hydrate crystallization in porous silica gel particles partially saturated with a surfactant solution. *Chem. Eng. Sci.* 98, 88–97.
- Duchateau, C., Pou, T.E., Hidalgo, M., Glénat, P., Dicharry, C., 2012. Interfacial measurements for laboratory evaluation of kinetic hydrate inhibitors. *Chem. Eng. Sci.* 71, 220–225.
- Freer, E.M., Sami Selim, M., Sloan, E.D., 2001. Methane hydrate film growth kinetics. *Fluid Phase Equilib.* 185, 65–75.
- Gayet, P., Dicharry, C., Marion, G., Gracia, A., Lachaise, J., Nesterov, A., 2005. Experimental determination of methane hydrate dissociation curve up to 55 MPa by using a small amount of surfactant as hydrate promoter. *Chem. Eng. Sci.* 60, 5751–5758.
- Gnanendran, N., Amin, R., 2004. Modelling hydrate formation kinetics of a hydrate promoter–water–natural gas system in a semi-batch spray reactor. *Chem. Eng. Sci.* 59, 3849–3863.
- Karanjkar, P.U., Lee, J.W., Morris, J.F., 2012. Surfactant effects on hydrate crystallization at the water–oil interface: hollow–conical crystals. *Cryst. Growth Des.* 12, 3817–3824.
- Kitamura, M., Mori, Y.H., 2013. Clathrate hydrate film growth along water/methane phase boundaries—an observational study. *Cryst. Res. Technol.* 48, 511–519.
- Kwon, Y.A., Park, J.M., Jeong, K.E., Kim, C.U., Kim, T.W., Chae, H.J., Jeong, S.Y., Yim, J. H., Park, Y.K., Lee, J.D., 2011. Synthesis of anionic multichain type surfactant and its effect on methane gas hydrate formation. *J. Ind. Eng. Chem.* 17, 120–124.
- Lee, S.Y., Kim, H.C., Lee, J.D., 2014. Morphology study of methane–propane clathrate hydrates on the bubble surface in the presence of SDS or PVCap. *J. Cryst. Growth* 402, 249–259.
- Li, S.L., Sun, C.Y., Liu, B., Feng, X.J., Li, F.G., Chen, L.T., Chen, G.J., 2013. Initial thickness measurements and insights into crystal growth of methane hydrate film. *AIChE J.* 59, 2145–2154.
- Li, S.L., Sun, C.Y., Liu, B., Li, Z.Y., Chen, G.J., Sum, A.K., 2014. New observations and insights into the morphology and growth kinetics of hydrate films. *Sci. Rep.* 4, 4129.
- Lin, W., Chen, G.J., Sun, C.Y., 2004. Effect of surfactant on the formation and dissociation kinetic behavior of methane hydrate. *Chem. Eng. Sci.* 59, 4449–4455.
- Lo, C.Y., Somasundaran, P., Lee, J.W., 2012. Quick assessment of potential hydrate promoters for rapid formation. *Geomaterials* 2, 63–69.
- Mitarai, M., Kishimoto, M., Suh, D., Ohmura, R., 2015. Surfactant effects on the crystal growth of clathrate hydrate at the interface of water and hydrophobic-guest liquid. *Crystal Growth and Design* (in press).
- Mochizuki, T., Mori, H.Y., 2006. Clathrate-hydrate film growth along water/hydrate-former phase boundaries-numerical heat transfer study. *J. Cryst. Growth* 290, 642–652.
- Ohmura, R., Shimada, W., Uchida, T., Mori, Y.H., Takeya, S., Nagao, J., Minagawa, H., Ebinuma, T., Narita, H., 2004. Clathrate hydrate crystal growth in liquid water saturated with a hydrate-forming substance: variations in crystal morphology. *Philos. Mag.* 84, 1–16.
- Okutani, K., Kuwabara, Y., Mori, Y.H., 2008. Surfactant effects on hydrate formation in an unstirred gas/liquid system: an experimental study using methane and sodium alkyl sulfates. *Chem. Eng. Sci.* 63, 183–194.
- Peng, B.Z., Dandekar, A., Sun, C.Y., Luo, H., Ma, Q.L., Pang, W.X., Chen, G.J., 2007. Hydrate film growth on the surface of a gas bubble suspended in water. *J. Phys. Chem. B* 111, 12485–12493.
- Peng, B.Z., Sun, C.Y., Peng, L., Liu, Y.T., Chen, J., Chen, G.J., 2009. Interfacial properties of methane/aqueous VC-713 solution under hydrate formation conditions. *J. Colloid Interface Sci.* 336, 738–742.
- Saito, K., Sum, A.K., Ohmura, R., 2010. Correlation of hydrate-film growth rate at the guest/liquid–water interface to mass transfer resistance. *Ind. Eng. Chem. Res.* 49, 7102–7103.
- Saito, K., Kishimoto, M., Ohmura, R., 2011. Crystal growth of clathrate hydrate at the interface between hydrocarbon gas mixture and liquid water. *Crystal Growth Des.* 11, 295–301.
- Salako, O., Lo, C., Couzis, A., Somasundaran, P., Lee, J.W., 2013. Adsorption of Gemini surfactants onto clathrate hydrates. *J. Colloid Interface Sci.* 412, 1–6.
- Servio, P., Englezos, P., 2003. Morphology of methane and carbon dioxide hydrates formed from water droplets. *AIChE J.* 49, 269–276.
- Sloan, E.D., Koh, C.A., 2008. *Clathrate Hydrates of Natural Gases*, 3<sup>rd</sup> edition CRC Press, Taylor and Francis Group, Boca Raton p. 712.
- Sun, Z.G., Ma, R.S., Wang, R.Z., Guo, K.H., Fan, S.S., 2003a. Experimental studying of additives effects on gas storage in hydrate. *Energy Fuels* 17, 1180–1185.
- Sun, Z.G., Wang, R.Z., Ma, R.S., Guo, K.H., Fan, S.S., 2003b. Natural gas storage in hydrates with the presence of promoters. *Energy Convers. Manag.* 44, 2733–2742.
- Sun, C.H., Chen, G.J., Ma, C.F., Huang, Q., Luo, H., Li, Q.P., 2007. The growth kinetics of hydrate film on the surface of gas bubble suspended in water or aqueous surfactant solution. *J. Cryst. Growth* 306, 491–499.
- Sun, C.Y., Peng, B.Z., Dandekar, A., Ma, Q.L., Chen, G.J., 2010. Studies on hydrate film growth. *Annu. Rep. Prog. Chem. Sect. C: Phys. Chem.* 106, 77–100.
- Tanaka, R., Sakemoto, R., Ohmura, R., 2009. Crystal growth of clathrate hydrates formed at the interface of liquid water and gaseous methane, ethane, or propane: variations in crystal morphologies. *Cryst. Growth Des.* 5, 2529–2536.
- Taylor, C.J., Miller, K.T., Koh, C.A., Sloan, E.D., 2007. Macroscopic investigation of hydrate film growth at the hydrocarbon/water interface. *Chem. Eng. Science* 62, 6524–6533.
- Uchida, T., Ebinuma, T., Kawabata, J., Narita, H., 1999. Microscopic observations of formation processes of clathrate-hydrate films at an interface between water and carbon dioxide. *J. Cryst. Growth* 204, 348–356.
- Veran-Tissoires, S., Prat, M., 2014. Evaporation of sodium chloride solution from a saturated porous medium with efflorescence formation. *J. Fluid Mech.* 749, 701–749.
- Wu, R., Kozielski, K.A., Hartley, P.G., May, E.F., Boxall, J., Maeda, N., 2013. Methane–propane mixed gas hydrate film growth on the surface of water and Luvicap EG solutions. *Energy Fuels* 27, 2548–2554.
- Zhang, B.Y., Wu, Q., Sun, D.L., 2008. Effect of surfactant Tween® on induction time of gas hydrate formation. *J. China Univ. Min. Technol.* 18, 18–21.
- Zhang, J., Lee, J.W., 2009. Enhanced kinetics of CO<sub>2</sub> hydrate formation under static conditions. *Ind. Eng. Chem. Res.* 48, 5934–5942.
- Zhang, J., Lo, C., Somasundaran, P., Lee, J.W., 2010. Competitive adsorption between SDS and carbonate on tetrahydrofuran hydrates. *J. Colloid Interface Sci.* 341, 286–288.
- Zhong, Y., Rogers, R.E., 2000. Surfactant effects on gas hydrate formation. *Chem. Eng. Sci.* 55, 4175–4187.
- Zhong, B.Y., Wu, Q., Sun, D.-J., 2008. Effect of surfactant Tween on induction time of gas hydrate formation. *J. China Univ. Min. Technol.* 18, 18–21.
- Zhong, D.L., Yang, C., Liu, D.P., Wu, Z.M., 2011. Experimental investigation of methane hydrate formation. *J. Cryst. Growth* 327, 237–244.